Polystyrene-*block*-poly(2-cinnamoylethyl methacrylate) Nanofibers—Preparation, Characterization, and Liquid Crystalline Properties

Guojun Liu,*[a] Jianfu Ding,[a] Lijie Qiao,[a] Andrew Guo,[a] Boris P. Dymov,[b] James T. Gleeson,[c] T. Hashimoto,[d] and K. Saijo[d]

Abstract: The two blocks of a polystyrene-*block*-poly(2-cinnamoylethyl methacrylate), PS-*b*-PCEMA, sample, with 1.25×10^3 styrene and 158 CEMA units, segregate in bulk films. PCEMA forms cylinders that disperse in the continuous matrix of PS when annealed at $110 \pm 2^\circ$C. UV photolysis cross-linked the PCEMA cylinders. Separating the cross-linked PCEMA cylinders by dissolving PS in toluene or THF yielded isolated nanofibers with PCEMA core and PS shell. Light scattering studies in toluene or chloroform revealed that the nanofibers were wormlike with a persistence length of ~ 400 nm, a molar mass exceeding 10^{10} g mol^{-1}, and a radius of ~ 43 nm. The nanofibers formed lyotropic liquid crystalline phases in bromoform and the order–disorder transition temperature of the liquid crystals increased with nanofiber concentration.

Keywords: block copolymers · nanofibers · nanostructures · self-assembly · supramolecular chemistry

Introduction

A diblock copolymer is a macromolecule consisting of two linear polymer chains joined together in a head-to-tail fashion. Polystyrene-*block*-poly(2-cinnamoylethyl methacrylate), PS-*b*-PCEMA, is a diblock copolymer. In this paper, we give a full description of a previously communicated method[1, 2] for the preparation of nanofibers from a PS-*b*-PCEMA sample containing 1.25×10^3 styrene and 158 CEMA units. We also report our new results on nanofiber characterization by light-scattering experiments and the lyotropic liquid crystalline properties of the nanofibers in bromoform.

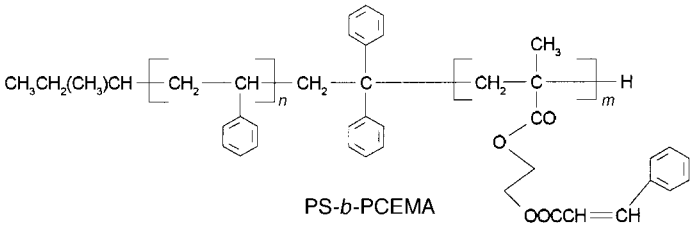

PS-*b*-PCEMA

Nanofibers in this paper are long cylinders with a cross-linked PCEMA core and PS shell. They are prepared by taking advantage of the self-assembling properties of the diblock in bulk and the photo-cross-linkability of PCEMA. The two blocks of a diblock copolymer, $(A)_n(B)_m$, segregate from one another in bulk owing to their incompatibility. The smallest dimension (radius for cylinders and thickness for lamellae) of a segregated A or B domain is similar to that of the individual A or B coils in a good solvent.[3–5] The shape of the A or B domain varies with the relative n and m values and the temperature. As the volume fraction of B increases gradually to $\sim 50\%$, the shape of the B domain normally changes from spheres ($\sim 17\%$) to cylinders ($\sim 28\%$), to gyroids ($\sim 38\%$), and finally to lamella ($\sim 50\%$). Domains with different shapes are formed to minimize the system's free energy. For preparing nanofibers, the PS-*b*-PCEMA sample was annealed at $110 \pm 2^\circ$C, so that PCEMA existed as cylinders dispersed in the continuous PS matrix. The PCEMA cylinders cross-linked upon photolysis. When separated from one another by dissolving PS in THF or toluene, the different cross-linked cylinders are dispersed as isolated "hairy" rods or nanofibers in dilute solutions.[1, 2]

Nanofibers here are similar in structure to diblock cylindrical micelles. Cylindrical micelles may form upon the

[a] Prof. G. Liu, Dr. J. Ding, Dr. L. Qiao, Dr. A. Guo
Department of Chemistry, University of Calgary
2500 University Dr., NW, Calgary, Alberta, T2N 1N4 (Canada)
Fax: (+1) 403 289-9488E-mail: gliu@acs.ucalgary.ca

[b] Dr. B. P. Dymov
Department of Physics, University of Calgary
Calgary, Alberta, T2N 1N4 (Canada)

[c] Prof. J. T. Gleeson[+]
Department of Physics, Kent State University
Kent, OH44242 (USA)

[d] Prof. T. Hashimoto, K. Saijo
Department of Polymer Chemistry, Kyoto UniversityKyoto 606 (Japan)

[+] Formerly in the Department of Physics, University of Calgary.

0947-6539/99/0509-2740 $ 17.50+.50/0 *Chem. Eur. J.* **1999**, *5*, No. 9

addition of a block-selective solvent into a concentrated diblock solution in a mutual solvent for the two blocks.[6–11] Alternatively, they can be prepared by levitating preformed cylinders out of a diblock solid with a solvent that selectively dissolves the matrix block.[12] The fundamental difference between our nanofibers and cylindrical micelles lies in their stability. While the nanofibers retain their structural integrity in all organic solvents, the cylindrical micelles are stable only in the solvent in which they are prepared and disintegrate in solvents that solubilize both blocks of a diblock. Cylindrical micelles may also undergo morphological transitions or change their aggregation number even in the same solvent by changing polymer concentration. The nanofibers have a similar structure as molecular "hairy rods",[13–16] which consist of a rigid polymer backbone with pendant, flexible alkyl side groups. The nanofibers are, however, much larger in size. They differ from cylindrical micelles of small-molecule surfactants[17] not only in size but also in their structural stability.

While the PS-*b*-PCEMA nanofibers prepared may not have immediate practical applications, the methodology utilized here is general and can be used for preparing nanofibers from other diblock copolymers. Nanofibers with appropriate chemical composition can, for example, be pyrolyzed[18, 19] to yield carbon, metal carbide, or silicon carbide nanofibers. Replacing the core block with a conductive polymer, one should be able to prepare nanowires with an insulating outer layer. The carbon, metal carbide, or silicon carbide nanofibers should be useful in nanocomposite preparation.[20, 21] The nanowire with an insulating layer, that is, the nanocable, should be useful in nanoelectronic devices.[22] While many methodologies exist for the preparation of carbon nanofibers,[21, 23–25] carbon nanotubes,[26–29] semiconductor nanowires,[29–31] and metal nanowires,[31] our methodology, like the electrospinning method,[32, 33] has the potential advantage for large-scale and cheap production of nanofibers.

Experimental Section

Polymer synthesis and characterization: The precursor to PS-*b*-PCEMA is PS-*b*-P(HEMA-TMS), where P(HEMA-TMS) denotes poly(2-trimethylsilylethyl methacrylate). PS-*b*-P(HEMA-TMS) was prepared by anionic polymerization as described in detail previously.[34–36] The TMS group hydrolyzed readily in methanol. Treatment of polystyrene-*block*-poly(2-hydroxylethyl methacrylate) with cinnamoyl chloride converted the HEMA groups quantitatively to CEMA, as revealed by NMR spectroscopic analysis. The sample was characterized by GPC, NMR spectroscopy, and light-scattering (LS) measurements; the characterization results of the polymer are shown in Table 1. From the ratios of the intensity of ^{1}H peaks of PS to those of PCEMA, the repeat unit ratio between PS and PCEMA, n/m, was determined to be 7.9. The GPC polydispersity index, $\bar{M}w/\bar{M}n$, of 1.12 in terms of PS standards suggests a narrow molar mass distribution. Using $n/m = 7.9$ and the LS molar mass of 1.71×10^5 g mol^{-1}, we obtained the weight-average n and m values of 1.25×10^3 and 1.58×10^2 for the sample.

Table 1. Characteristics of the PS-*b*-PCEMA sample used.

n/m from NMR	$\bar{M}_w/\bar{M}_n$ from GPC	$10^{-4}\,\bar{M}_w$ [g mol^{-1}] GPC	$10^{-4}\,\bar{M}_w$ [g mol^{-1}] LS	$10^{-2}n$	$10^{-2}m$
7.9	1.12	15	17.1	12.5	1.58

Bulk films or disks: PS-*b*-PCEMA solid films or disks, 1 to 4 mm thick, were prepared by evaporating ~20% (by mass) polymer solution in toluene in polyethylene bottles or capsules over three to four days. The films were then annealed at 60 ± 5°C under 30 cm Hg pressure for another three days and then at 110 ± 2°C for three weeks. Two circular disks with a thickness of 1.5 mm and a diameter of ~12 mm were used for small-angle X-ray scattering (SAXS) studies. Measurements were carried out with $Cu_{K\alpha}$ radiation ($\lambda = 0.154$ nm) from a 18 kW rotating anode generator (MAC Science, Yokohama, Japan). For examining PCEMA cylinder orientation, two-dimensional imaging plates, 1.4 m away from a sample were used to obtain the X-ray diffraction patterns. In the through-scattering mode, the diffraction pattern was obtained by using a point-collimated X-ray beam impinging at the center of a diblock disk along the disk normal. In the edge-scattering mode, a rectangular strip of the size of $4 \times 3 \times 1.5$ mm^3 was cut from the center of the disk, and the incident beam struck the sample along the direction parallel to the sample surface.[37]

Nanofiber preparation: PS-*b*-PCEMA bulk films that had been annealed at 110 ± 2°C for three weeks were irradiated for 40 min, on each side, with UV light filtered through a 310 nm cut-off filter. The films were irradiated on different sides at the tail of the PCEMA absorption peak rather than at its maximum at 274 nm to achieve uniform CEMA cross-linking across the whole film thickness. After photolysis, the films were immersed in THF and stirred. The films swelled and disintegrated in one day. Such a solution was centrifuged to remove the insoluble product. The supernatant, which had a bluish tinge, was concentrated and precipitated into methanol to yield nanofiber powders with ~50% yield. FTIR spectroscopic measurements were carried out with both the THF-soluble and THF-insoluble products in the powder form in order to estimate the PCEMA double-bond conversion.

TEM studies: Bulk samples were divided by ultramicrotomy (Ultracut-E, Reichert-Jung) into slices with a thickness of ~50 nm. The divided samples were stained with OsO_4 vapor overnight before being viewed under a Hitachi-7000 electron microscope (TEM) operated at 100 kV. For TEM studies of the nanofibers, a dilute nanofiber solution in THF was spread on a water surface. The nanofiber film formed was then transferred onto a carbon-coated copper grid and stained by OsO_4 vapor.

Light-scattering studies of nanofibers: Nanofibers were purified for light-scattering study. The crude product (15 mg) was dissolved in THF (~0.5 mL). Cyclopentane was added to a volume fraction of ~80%. The nanofibers were then centrifuged and separated from the supernatant, which contained some low molar mass material. The nanofibers were dissolved in THF again. After filtration through tightly-packed glass wool to remove large dust particles, the nanofibers were precipitated into filtered methanol, centrifuged, and dried. Light-scattering studies were performed with a Brookhaven model 9025 instrument equipped with an Argon ion laser operated at 488 nm. Purified nanofibers were dissolved in spectrograde toluene or chloroform that had passed through a 0.2 μm filter to yield the desired concentration. Light intensities were measured for such samples at different dilution at the scattering angles, θ, of 16, 18, 21, 24, 27, 30, 33, 36, 40, 50, 60, 70, 80, 90, 100, 110, 120, 130, and 140°. Light-scattering measurements were performed for samples at three sets of concentrations in toluene and one set of concentrations in chloroform. The highest and lowest concentrations used in a given experiment with five samples differ typically by a factor of 4 to 6. The highest concentrations used in the three sets of experiments carried out in toluene were 3.55×10^{-3}, 1.20×10^{-3}, and 0.18×10^{-3} g mL^{-1}, respectively, and that in chloroform was 2.55×10^{-3} g mL^{-1}. Light-scattering experiments for samples with relatively high nanofiber concentrations were tricky, because instrument settings suitable for nanofiber solution study gave a negligible scattering intensity from toluene, the calibration solvent. This difficulty was circumvented by measuring the scattered intensities of toluene and the nanofiber solutions in the absence and presence of a neutral density filter placed in the incident beam. The instrument calibration constant thus obtained from toluene was subsequently corrected by taking the optical transmission of this filter at 488 nm into account.

Studies of the liquid crystalline properties of the nanofibers: Nanofibers were mixed with distilled bromoform. This mixture was gently warmed until a transparent and uniform solution was formed. As the solvent evaporated, the solution weight was monitored until the desired concentration was reached. At high concentrations, the solution was gel-like. An aliquot of this solution was deposited in the well of a culture slide. For

shearing a sample, a stainless-steel spatula was pressed down on the sample and was used to "smear" it, with a pressure of about 3 MPa, in the same fashion that one applies jam to bread. The slide was then sealed against further evaporation of the solvent. The liquid crystalline properties were studied by using an optical microscope equipped with polarizers and a heating stage.

PCEMA density determination: A ~20%, by mass, of PCEMA solution in toluene was cast on a glass slide. The film was dried at room temperature for one day and at 110°C under vacuum for another day. The film was then cut into five pieces each of which was 9 mm^2 large and 1 mm thick. The small pieces were placed in a 8 mL vial with $CaCl_2$ (0.9909 g). Water was gradually added into the vial under stirring. At the critical point when the PCEMA films were to about settle but were still suspended water addition was stopped, and the total amount of water added was determined to be 4.16 g. The density of the final aqueous solution at this stage at 20°C was found from a handbook[38] to be 1.25 $g\,cm^{-3}$; this is assumed to be the same as that of PCEMA.

Results and Discussion

This section starts with TEM results demonstrating PCEMA cylinder formation in a PS matrix. Information on the orientation of the cylinders is obtained from SAXS results. Following evidence for nanofiber preparation, the nanofiber characterization results from light-scattering experiments are presented. This section finishes with the report of the liquid crystalline properties of the nanofibers in bromoform.

Morphologies of block-segregated PS-*b*-PCEMA films: The density of PCEMA is 1.25 and that of PS is 1.05 $g\,cm^{-3}$.[39] Using these densities and $n/m = 7.9$, we obtained a volume fraction of 21% for PCEMA. At this volume fraction, the equilibrium PCEMA domain shape should be between spheres and cylinders.[3–5] Figure 1 illustrates a representative TEM image obtained of thin slices of PS-*b*-PCEMA annealed at 110 ± 2°C, which is above the glass transition temperatures of 69 and 101°C for PCEMA[40] and PS.[39] Since the TEM specimens were stained with OsO_4, which should react selectively with PCEMA, the PCEMA regions should appear darker. The dark circles in Figure 1 must represent PCEMA cylinders pointing out of the picture. The dark ellipses may represent cylinders lying slightly off the electron-beam direction. The radius of the PCEMA cylinders, r_{CEMA}, estimated from the dark circles, is ~13 nm.

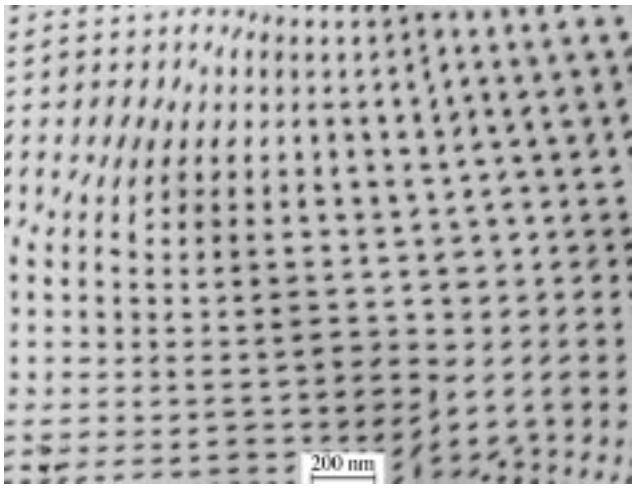

Figure 1. TEM image of a 50 nm thick PS-*b*-PCEMA slice. The sample was dried at room temperature for three days and annealed under 30 cm Hg pressure at 65 ± 5°C for three days and 110 ± 2°C for three weeks.

The cylinders in Figure 1 are, however, not packed with hexagonal symmetry. Rather, the cylinders are packed rectangularly. The short and long sides, D_s and D_L, for the rectangles are ~45 and ~57 nm, respectively. A rectangular unit cell should contain one PCEMA cylinder with its cross-sectional area given by πr_{CEMA}^2. The total cross-sectional area of a unit cell is $D_L \times D_S$. This gives a PCEMA cross-sectional area ratio or volume fraction of 0.21. This is in exact agreement with the value calculated from $n/m = 7.9$ and the densities of PS and PCEMA. This agreement supports the cylindrical morphology for PCEMA.

The rectangular packing of the cylinders is surprising. This might be an effect of shearing from the microtoming process. To shed light on this phenomenon, SAXS studies were performed. Figure 2 displays two-dimensional X-ray diffraction patterns obtained for a sample in both the edge- and through-scattering modes. The intensity and the halos obtained in the through-scattering mode have approximately circular symmetry. This suggests no preferential orientation of the PCEMA cylinders in the disk plane on the size scale of the X-ray beam cross-sectional area, $0.25 \times 0.25\ mm^2$, despite their ordering in grains of the size of micrometers, as probed by TEM. The diffraction pattern obtained in the edge-scattering mode is, however, not circularly symmetric, and stronger scattering is observed along the horizontal direction. This indicates that the PCEMA cylinders lie preferentially in the plane of the disk. The primary peaks along the horizontal direction of the SAXS are further away than those along the vertical direction. This suggests that the spacing of the cylinders that lie in the cylinder plane is smaller than that normal to disk surface. This is a nonequilibrium effect encountered frequently in solution-cast samples.

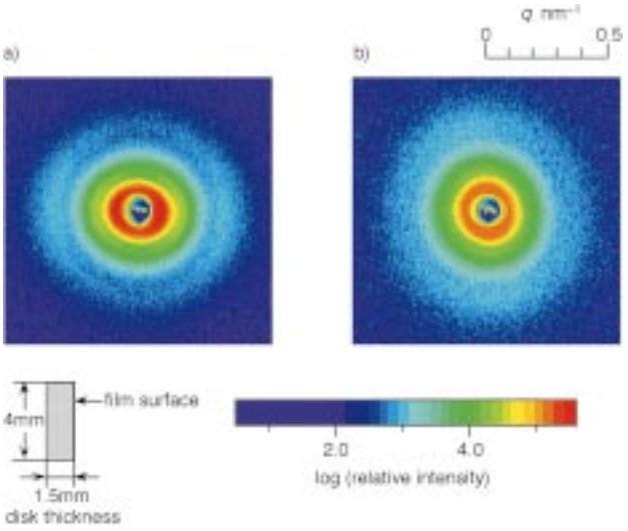

Figure 2. Edge (left) and through (right) two-dimensional small-angle X-ray diffraction patterns obtained for a PS-*b*-PCEMA disk annealed at 110 ± 2°C for three weeks.

Owing to the circular symmetry of the through-scattering pattern shown on the right of Figure 2, its averaged circular intensities are plotted in Figure 3 as a function of q_x, the

0947-6539/99/0509-2742 $ 17.50+.50/0 *Chem. Eur. J.* **1999**, *5*, No. 9

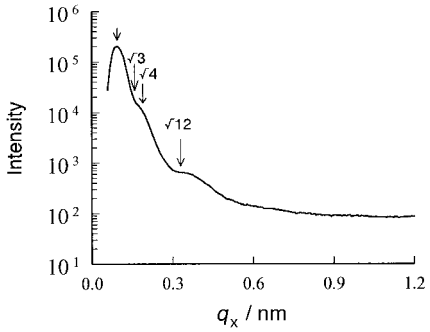

Figure 3. Plot of scattered X-ray intensity as a function of the magnitude of the scattering wave vector, q_x. The intensities are the averages over circles with different distances from the center of diffraction pattern shown on the right of Figure 2.

magnitude of the scattering wave vector [Eq. (1)]. In Equation (1) $2\theta_x$ is the scattering angle and $\lambda = 0.154$ nm is the wavelength of the X-ray used.

$$q_x = \frac{4\pi}{\lambda} \sin\theta_x \qquad (1)$$

The first-order peak occurs at $q_o = 0.094\ \mathrm{nm}^{-1}$. The higher-order peaks are broad and do not necessarily occur at the positions expected of hexagonally packed cylinders. Thus, the cylinders may have inherent nonhexagonal packing in agreement with the TEM results. The broadness of the peaks suggests that there is a wide distribution in the inter-cylinder distances.

A more quantitative description of the cylindrical morphology was obtained by analyzing the experimental SAXS profile (Figure 3) with an equation derived from a paracrystal model.[41, 42] This model assumes that 1) the aspect ratio of the cylinders is large, 2) the cylinders are packed parallel to each other with hexagonal symmetry in micrometer-sized grains, 3) the orientation of the grains is random, and 4) the interface between the P*t*BA and PCEMA domains is sharp. Parameters used in the curve-fitting equation are the mean closest neighbor distance D (78 nm), with a standard deviation ΔD (9.8 nm), and the mean radius of the cylinders R (14.5 nm), with a standard deviation ΔR (2.5 nm). From $(2\pi\sqrt{3})(R/D)^2$, the volume fraction of the P*t*BA domain was determined to be 0.125, a value lower than the volume fraction (0.21) obtained from TEM and mass-fraction calculations. The difference between 0.125 and 0.21 and the large ΔR and ΔD values again point to nonhexagonal cylinder packing.

In order to obtain hexagonal cylinder packing, we annealed the samples at higher temperatures. Figure 4 illustrates a TEM image of a sample annealed at $135 \pm 2^\circ$C for three weeks. The pattern shown was not localized but found throughout the sample, and the observation was reproducible. The PCEMA block seems to form crossed cylinders here. After annealing at $145 \pm 10^\circ$C for one week, TEM images as shown in Figure 5 were obtained. PCEMA seems to form spherical domains dispersed in the PS matrix and the spheres have irregular packing with a wide size distribution. Thus, hexagonal packing could not be obtained by annealing the samples at higher temperatures.

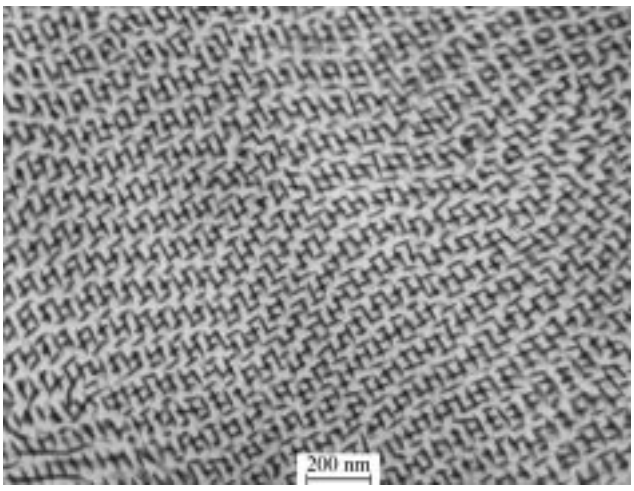

Figure 4. TEM image of a 50 nm thick PS-*b*-PCEMA slice. The sample was dried at room temperature for three days and annealed under 30 cm Hg pressure at $65 \pm 5^\circ$C for three days and $135 \pm 2^\circ$C for three weeks.

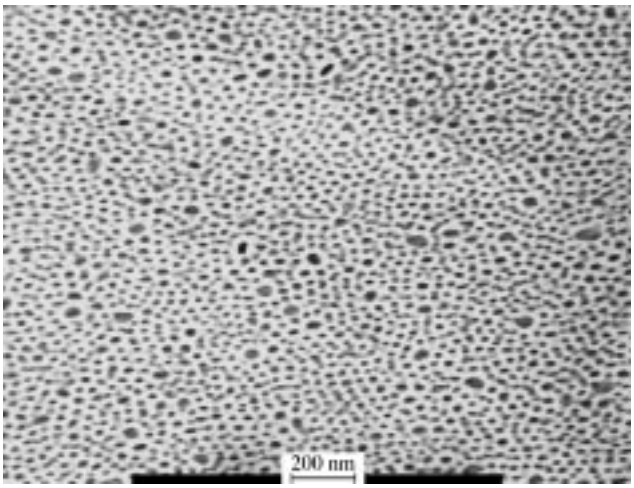

Figure 5. TEM image of a 50 nm thick PS-*b*-PCEMA slice. The sample was dried at room temperature for three days and annealed under 30 cm Hg pressure at $65 \pm 5^\circ$C for three days and $145 \pm 2^\circ$C for one week.

The formation of spherical PCEMA domains at 145°C is reasonable for the PCEMA volume fraction of 21%.[3–5] However, we do not know the reason for the observation of the seemingly new "crossed-cylinder" morphology at 135°C or for the wide distribution in the sizes of the spheres at 145°C. The answers to these question were not further pursued because of the limited scope of this research.

Locking in the PCEMA domains: CEMA dimerizes as a result of photo-induced cyclo-addition of the double bonds.[43, 44] The dimerization can occur between two CEMA units of the same chain, which does not effect structural "locking in" of the cylinders. PCEMA cross-links because of dimerization between CEMA groups of different chains in the cylinders. Owing to the expected high degree of PCEMA inter-chain mixing, the cross-linking process should be effective. In fact, PCEMA photo-cross-linking has been used by us to prepare a wide range of nanostructures including nanospheres,[35, 45, 46] cross-linked polymer brushes (monolayers),[47] and nanochannels in polymer thin films.[48, 49]

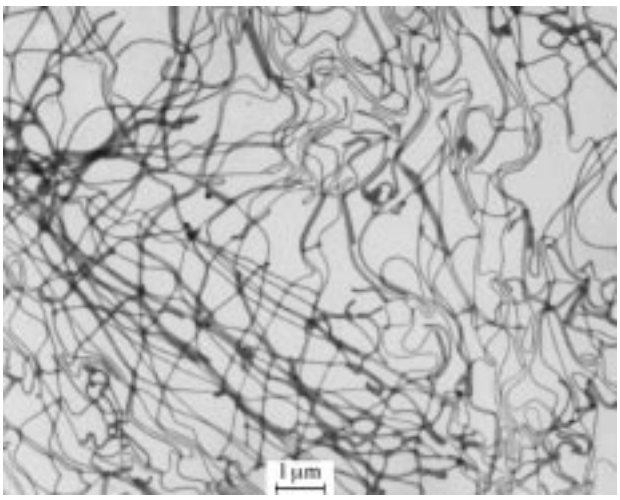

Figure 6. TEM image of nanofibers. To prepare the TEM sample, a drop of a dilute toluene solution was dispensed on water surface, and the solvent was allowed to evaporate. The nanofiber, thin film formed was then transferred onto a carbon-coated copper grid and was stained by OsO_4.

The locking in of the PCEMA domains is unambiguously demonstrated by the stability of the nanofibers in THF, a solvent which dissolves both PS and uncross-linked PCEMA. Figure 6 illustrates a TEM image of the nanofibers. They have a narrow width, but a relatively wide length distribution. They are wormlike and can be tens of micrometer long.

The cross-linking of PCEMA can also be appreciated from the FTIR spectroscopic results shown in Figure 7. UV irradiation substantially reduced the carbon – carbon double-bond peak intensity at 1635 cm^{-1}. At the PS-*b*-PCEMA film thickness of ~0.5 mm, the PCEMA double-bond conversions are 18 % and 22 % after the films were irradiated on each side for 20 and 40 minutes, respectively. The nanofibers used in this study had a CEMA conversion of 22 %.

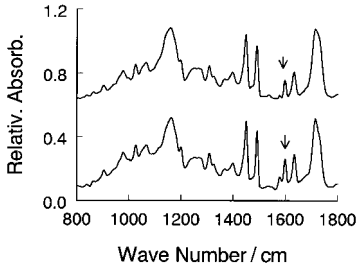

Figure 7. Comparison between FTIR spectra of PS-*b*-PCEMA (bottom) and the nanofibers (top). The 1635 cm^{-1} peaks are marked with arrows.

Figure 8 shows a magnified view of a small area in Figure 6. Evidently, the nanofibers here have a dark core and a gray shell. Since PCEMA was selectively stained, the core must be made up of PCEMA, as expected. The diameter of the core as measured from Figure 8 is ~26 nm, which is the same as that determined for the PCEMA cylinders in Figure 1. The diameter of the fiber including the shell is ~92 nm. Since the volume fraction of PCEMA is 21 %, the diameter of a dry, cylindrical nanofiber, calculated from the PCEMA core

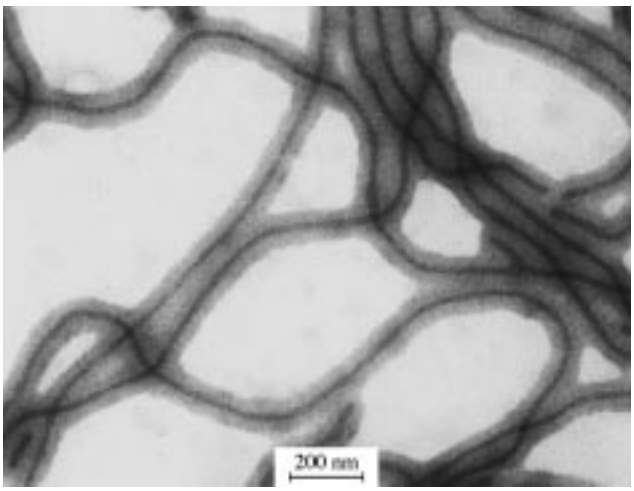

Figure 8. A close-up view of a small area of the sample shown in Figure 6.

diameter of ~26 nm, should be ~57 nm. The much larger diameter suggests that the PS chains were substantially flattened on water surfaces on which the TEM samples were prepared. This is reasonable because the PS chains would not stretch below the water surface owing to their hydrophobicity.

Light-scattering results: The TEM image of Figure 6 gives an idea of the conformations of "dry" nanofibers. Their conformations in solution were probed by light-scattering experiments. Light-scattering measurements were performed in either toluene or chloroform. In each experiment, five polymer concentrations were used. Figure 9 shows plots of

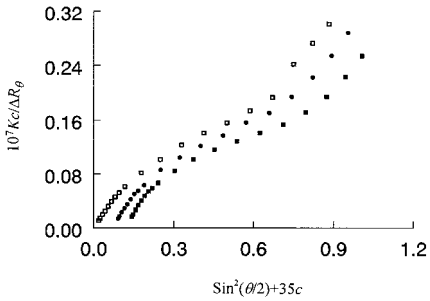

Figure 9. Plot of $Kc/\Delta R_\theta$ vs. $\sin^2(\theta/2)+35c$ for nanofibers in toluene. Data were obtained at five nanofiber concentrations and those for the concentrations of 3.55×10^{-3} (■) and 2.06×10^{-3} (●) are shown. Also shown are the $Kc/\Delta R_\theta$ values (□) obtained by extrapolating to zero nanofiber concentration.

the $Kc/\Delta R_\theta$ versus $[\sin^2(\theta/2)+35c]$ data obtained for nanofibers in toluene at the concentrations of 3.55×10^{-3} and 2.06×10^{-3} g mL^{-1}, whose K is the optical constant, ΔR_θ is the excess Rayleigh ratio, θ is the scattering angle, and c is the nanofiber concentration in g mL^{-1}. Also shown are the $Kc/\Delta R_\theta|_{c\to0}$ data obtained by extrapolating the $Kc/\Delta R_\theta$ data at five concentrations to zero nanofiber concentration at each angle. Similar $Kc/\Delta R_\theta|_{c\to0}$ data were obtained for the nanofibers in toluene when the extrapolation was performed for nanofiber samples about 20 times more dilute or when the experiment was carried out in chloroform. The $Kc/\Delta R_\theta|_{c\to0}$ versus $\sin^2(\theta/2)$ line is curved, suggesting the large size of the nanofibers.

0947-6539/99/0509-2744 $ 17.50+.50/0 *Chem. Eur. J.* **1999**, *5*, No. 9

Owing to the nanofiber size, such data should not be treated following the Zimm method.[50] Instead, the $Kc/\Delta R_\theta$ data are analyzed by the more general relation given in Equation (2),

$$\frac{Kc}{\Delta R_\theta}=\frac{1}{M_w P(\theta)}+2A_2c \tag{2}$$

in which $P(\theta)$, the particle structure factor or scattering function, is a function of the relative positions of the different units in the particle being analyzed. If a particle consists of n_s sub-units, which are much smaller than the wavelength of light, with ith and jth sub-units separated by distance h_{ij}, $P(\theta)$ is given by Equation (3).[50] In Equation (3), $P(q)$ is replaced by $P(\theta)$, because the magnitude of the scattering wave-vector q is related to the scattering angle θ by the relation shown in Equation (4).

$$P(\theta)=\frac{1}{n_s^2}\sum_{i=1}^{n_s}\sum_{j=1}^{n_s}\frac{\sin qh_{ij}}{qh_{ij}} \tag{3}$$

$$q=\frac{4\pi n_r}{\lambda}\sin(\theta/2) \tag{4}$$

In Equation (4), n_r, the refractive index of toluene, is 1.496, and λ, the wavelength of the laser light used, is 488 nm. Equation (2) can be simplified by extrapolating to zero concentration to yield Equations (5) or (6).

$$\frac{Kc}{\Delta R_q}\Big|_{c\to 0}=\frac{1}{M_w P(q)} \tag{5}$$

$$\bar{M}_w P(q)=\frac{\Delta R_q}{Kc}\Big|_{c\to 0} \tag{6}$$

Since $\bar{M}_w$ is a constant for a given sample, $\Delta R_q/Kc\,|_{c\to 0}$ defines the shape of the particle structure function, $P(q)$. As $P(q)$ can be calculated based on an assumed shape for the particle, the comparison between $\Delta R_q/Kc\,|_{c\to 0}$ and theoretical $P(q)$ functions provides a means for checking the conformation of the nanofibers in solution and for determining the molar mass $\bar{M}_w$.

$\Delta R_q/Kc\,|_{c\to 0}$ data analysis by the wormlike-thread model: The TEM image in Figure 6 suggests that the nanofibers are long wormlike threads with a persistence length b upto submicrometers. We started by treating the $\Delta R_q/Kc\,|_{c\to 0}$ data with the wormlike-thread model by assuming a nanofiber contour length of L and hydrodynamic radius R.

There have been numerous studies, including those exemplified in refs. [51–53], of scattering functions of wormlike threads with an infinitely thin cross-section. Such studies normally involved the evaluation of $P_{thin}(q)$ by using Equation (3) and segment distribution functions established either theoretically[51, 52] or from Monte Carlo simulations.[53] The resultant $P_{thin}(q)$ expressions are generally complex and difficult to handle in data treatment. More recently, Pedersen and Schurtenberger[53] fitted $P_{thin}(q)$ generated from Monte Carlo simulations with expressions containing relatively few terms. Their $P_{thin}(q)$ will be used in treating our experimental data.

The $P_{thin}(q)$ functions used by Pedersen and Schurtenberger[53] consisted of two parts. One part, $P_{SF}(q)$, is responsible for the semi-flexible coil behavior[52] on size scales larger than b or $qb<2$ and is given in Equation (7), in which $u=q^2(Lb/6)^2$.

$$P_{SF}(q)=\frac{2[\exp(-u)\ +\ u-1]}{u^2}+\left[\frac{4}{15}+\frac{7}{15u}-\left(\frac{11}{15}+\frac{7}{15u}\right)\exp(-u)\right](b/L) \tag{7}$$

The other part, $P_{Loc}(q)$, is derived from the rodlike structure of wormlike chains on scales comparable or smaller than b or $1<qb<10$ [Eq. (8)]. The semi-flexible to rigid rod transition in the scattering function is made by modifying the two parts

$$P_{loc}(q)=\frac{1}{Lqb^2}+\frac{\pi}{Lq} \tag{8}$$

with exponential functions so that $P_{SF}(q)$ and $P_{loc}(q)$, respectively, contribute decreasingly and increasingly more towards $P_{thin}(q)$ as q increases [Eq. (9)].

$$P_{thin}(q)=P_{SF}(q)\exp[-(qb/q_1)^{p_1}]+P_{Loc}(q)\{1-\exp[-(qb/q_1)^{p_1}]\} \tag{9}$$

The fitting of $P_{thin}(q)$, generated from Monte Carlo simulations of chains with different L and b to satisfy $L/b>2$ and $qb<10$ with Equation (9), established that $p_1=5.33$ and $q_1=5.53$.

Our nanofibers have a finite cross-section with a core-shell structure just like that of cylindrical surfactant micelles. Jerke et al.[54] developed the cross-section scattering functions of such micelles by taking the different scattering contrast of the core and shell into consideration. As will be evident later, the q range of our light-scattering data is narrow and would not justify the use of such a sophisticated model containing many fitting parameters, which include the core radius, shell radius, core refractive index, and shell refractive index. Thus, we assume that our nanofiebrs have a homogeneous cross section with a hydrodynamic radius R. The scattering function for such a cross section is given in Equation (10), in which $J_1(Rq)$, the first-order Bessel function of the first kind, is given by Equation (11). The overall scattering function for the nanofibers is then given by Equation (12), with L, b, and R as the variables.[53]

$$P_{CS}(q)=\left[\frac{2J_1(Rq)}{Rq}\right]^2 \tag{10}$$

$$J_1(Rq)=\sum_{i=0}^{\infty}\frac{(-1)^n}{n!(n\ +\ 1)!}\left(\frac{Rq}{2}\right)^{2n+1} \tag{11}$$

$$P(q)=P_{thin}(q)P_{CS}(q) \tag{12}$$

Two sets of $P(q)$ functions are displayed in Figure 10, with L and R fixed at 20 μm and 50 nm and with b equal to 200 and 400 nm, respectively. The data are presented by following the Holtzer method, that is, $qP(q)$ rather than $P(q)$ is plotted against q, so that the different regions of $P(q)$ are more clearly seen. $qP(q)$ initially increases with q, because the Guinier region, in which $P(q)$ changes slowly with q, associated with the overall size of the fiber is observed. After reaching a maximum, $qP(q)$ decreases because $P(q)$ crosses over to a power-law dependence on q. This region is characteristic of the coil behavior of the fibers with an exponent of -2 in theta solvent and $-5/3$ in good solvent. For the set of data generated with $b=400$ nm, a flat region is seen after $q=0.01$ nm^{-1}. This is characteristic of the local stiffness of the

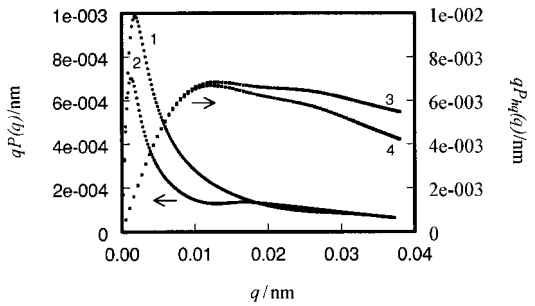

Figure 10. Curves of $qP(q)$ and $qP_{hq}(q)$ as a function of q. Curves 1 and 2 were constructed by using $L = 20$ μm, $R = 50$ nm, and b values of 200 and 400 nm, respectively. While $l = 400$ nm, the R values are 30 and 40 nm for curves 3 and 4, respectively.

chain and of $P(q) \propto 1/q$. $qP(q)$ further decreases with q at even higher q values because of the Guinier scattering behavior of the cross-section of the nanofibers.

A broad and small peak is seen at $q = 0.18$ nm^{-1} for $qP(q)$ generated by using $L = 20$ μm, $R = 50$ nm, and $b = 400$ nm. We have examined systematically how changing L, b, and R affected the shape of $qP(q)$. Increasing L and b shifted the maximum of $qP(q)$ to lower q values. Increasing R made $qP(q)$ decrease more sharply in the high q region. This systematic study also suggested that the broad and small peak in the $qP(q)$ curve was due to the empirical nature of Equation (12) and the error associated with the large qb of 7.2.

The experimental $q(\Delta R_\theta/Kc)_{c\to 0}$ values are illustrated in Figure 11. The presence of few data points in the high q region that suggests the downward bending of $qP(q)$ justifies our previous adoption of the simplified cross-section model for

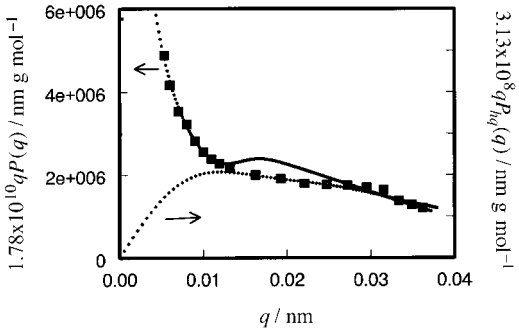

Figure 11. Comparison between $1.78 \times 10^{10} qP(q)$ (●) or $3.13 \times 10^8 qP_{hq}(q)$ (◆) and experimental $\Delta R_\theta/Kc\,|_{c\to 0}$ data (■). The $qP(q)$ and $qP_{hq}(q)$ functions are valid only in the low and high q regions, respectively. The $qP(q)$ function was generated by assuming $L = 20$ μm, $R = 50$ nm, and $b = 400$ nm. The $qP(q)$ function was obtained by using $l = 400$ nm and $R = 43$ nm.

nanofibers. More data points are also needed at the low q end so that the $qP(q)$ maximum can be located for an accurate determination of both L and b. Because of the narrow q region probed, the results obtainable from any data treatment procedure cannot be more than qualitative. For this, we took a crude approach by fixing L at 20 μm and R at 50 nm and examined the results to see if a reasonable b value could be obtained. The contour length of 20 μm should be reasonable as judged from Figure 6. As will be shown later, the R value of 50 nm is reasonable as well. Furthermore, the choice of R values only affects the $qP(q)$ shape in the high q region where Equation (12) is not valid.

Also shown in Figure 11 is the comparison between the experimental $q(\Delta R_\theta/Kc)_{c\to 0}$ values and 1.78×10^{10} (g mol^{-1}) $\times$ $qP(q)$ with $qP(q)$ calculated from Equation (12) with $L = 20$ μm, $R = 50$ nm, and $b = 400$ nm. The agreement in the low and high q regions is excellent. The discrepancy in the intermediate region is probably due to error inherent in Equation (12) at large qb values.

The good agreement between 1.78×10^{10} (g mol^{-1})$qP(q)$ and $q(\Delta R_\theta/Kc)_{c\to 0}$ in the high q region is fortuitous as Equation (12) can be erroneous for $qb > 10$. The agreement in the low q region suggests that the persistence length of the nanofibers is $\sim$400 nm; a result in qualitative agreement with what one deduces from Figure 6. According to Equation (6), the molar mass of the nanofiber should be 1.78×10^{10} g mol^{-1}. The molar mass of the nanofibers can also be calculated from the contour length L of 20 μm by using Equation (13), in

$$\bar{M}_w = N_A \rho_{CEMA} \pi r^2_{CEMA} L / W_{CEMA} \tag{13}$$

which N_A is Arvogadro's number; ρ, density of PCEMA, is 1.25 g cm^{-3}; W_{CEMA}, the weight fraction of PCEMA, is 0.24; and r_{CEMA}, the radius of PCEMA core, is $\sim$13 nm as revealed from Figure 1. The molar mass of 3.33×10^{10} g mol^{-1} calculated from Equation 13 is in qualitative agreement with 1.78×10^{10} g mol^{-1}, suggesting the validity in the choice of the L value.

$\Delta R_q/Kc\,|_{c\to 0}$ data analysis in the high q region: As a result of the break down of Equation (12) in the high q region, the data were treated differently in this region to obtain the cross-sectional hydrodynamic radius of the nanofibers in toluene. In the high q region, the nanofibers essentially behave as rigid rods with length l approximately equal to the persistence length b and so the rigid-rod model was used. For randomly oriented, cylindrical rigid rods with a radius R, length l, and $l/R \gg 1$, Equation (14) can be derived for $P_{hq}(q)$,[55, 56] in which $J_1(qR\sin\beta)$ is again the first-order Bessel function of the first kind. The second term in the square bracket on the right-hand side denotes the contribution from the cross-section to the scattering function.

$$P_{hq}(q) = \int_0^{\pi} 2\left[\frac{\sin(ql\cos\beta/2)}{ql\cos\beta/2}\frac{J_1(qR\sin\beta)}{qR\sin\beta}\right]^2 \sin\beta \mathrm{d}\beta \tag{14}$$

Equation (14) is clearly a function of l and R. In Figure 10 two sets of $P_{hq}(q)$ curves are compared that were generated by using $l = 400$ nm, $R = 30$, 40 nm. As R increases, the $P_{hq}(q)$ curve bends downward more sharply at the high q end, but is not affected at the low q end. We also examined the effect of varying l on the shape of the $P_{hq}(q)$ curve. Increasing l decreased the height of the $P_{hq}(q)$ curve and shifted the position of the first bending point in the curve to lower q values. Since the analysis here is only qualitative owing to the narrow q range probed, we set l equal to the persistence length b obtained from the wormlike-thread model, that is, $l = 400$ nm. At this fixed l value, good agreement between the experimental $q(\Delta R_q/Kc)_{c\to 0}$ values and $P_{hq}(q)$ is obtained by setting $R = 43$ nm and $\bar{M}_w = 3.13 \times 10^8$ g mol^{-1}. This $\bar{M}_w$ is very

0947-6539/99/0509-2746 $ 17.50+.50/0 Chem. Eur. J. 1999, 5, No. 9

reasonable for a 400 nm rod considering that the molar mass for a 20 μm rod is $1.78 \times 10^{10}\,g\,mol^{-1}$ from the wormlike-thread model.

Although not shown here, the light-scattering data of the nanofibers in chloroform can also be fitted by use of the same models to yield $L = 20$ μm, $b = 400$ nm, and $R = 43$ nm. The R value of 43 nm is substantially larger than 28 nm, the radius estimated for dry nanofibers, but smaller than the TEM radius of 46 nm determined from Figure 8. It is larger than 28 nm, because the nanofiber chains are swollen in toluene or chloroform. On water surfaces the nanofibers are flattened; this makes the TEM radius larger than that in the organic solvents. Thus, the value of 43 nm is very reasonable. However, we will treat 43 nm only as a semi-quantitative value owing to the various assumptions associated with its determination and no further discussion will be made about its implications.

Liquid crystalline properties of the nanofibers: The TEM images in Figures 6 and 8 suggest that the dry nanofibers are quite rigid. They are also quite rigid in toluene or chloroform, as confirmed by their large persistence length. As a result of their rigidity and the large b/R value, the Onsager theory[57] for "hard rods" and the Semenov and Kohhlov theory[58] for semi-flexible rods predict that the nanofibers should have liquid crystalline properties. We examined the optical birefringence of such nanofibers in bromoform by means of polarized optical microscopy.

The nanofiber solutions as prepared in bromoform showed little or no birefringence, an indication of the absence of long-range orientation order. However, the optical birefringence or nanofiber ordering developed upon gel shearing. Figure 12 is a photomicrograph, taken through crossed polarizers, of a 42.5% by weight solution of the nanofibers in bromoform. The central region looks brighter, because a spatula was used to smear the sample across this region. Such birefringence persisted until the sample was heated above a critical temperature as shown in Figure 13, in which the variation in the intensity of light transmitted through crossed polarizers is plotted as a function of temperature. As the temperature increased, the intensity initially stayed constant and then decreased suddenly until the birefringence essentially disappeared. This suggests an order–disorder transition for the nanofibers. Unfortunately, this transition is not reversible, because the birefringence of a sample heated above its order–disorder transition temperature returns only very weakly if at all.

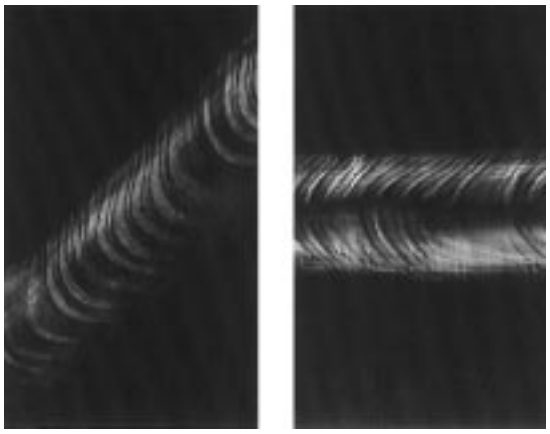

Figure 12. Micrographs taken through crossed polarizers a 42.5 wt% solution sample of nanofibers in bromoform smeared with a spatula. The right-hand picture was taken at a position with the shearing direction parallel to the analyzing polarizer axis. The left-hand picture was taken after the sample stage was rotated by 45°. The width of each frame in the figure is about 5 mm.

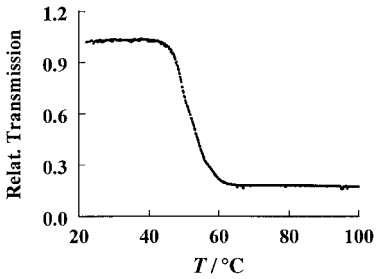

Figure 13. Variation in the transmitted light intensity through crossed polarizers, with a 42.5% nanofiber solution between them, as a function of temperature.

The order–disorder transition temperature has been defined the temperature at which the transmitted light intensity drops half way between its low and high temperature values. The variation in the transition temperature as a function of nanofiber concentration in bromoform is plotted in Figure 14. As nanofiber concentration increases, the transition temperature increases.

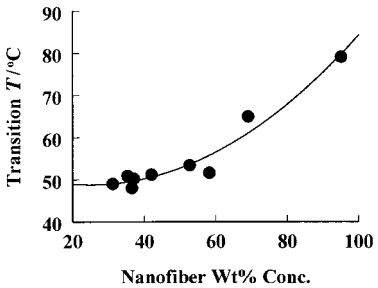

Figure 14. Plot of variation in order-disorder transition temperature (●) as a function of nanofiber concentration in bromoform. The solid line represents the best fit to experimental data by a second-order polynomial.

Birefringence development under shearing: Since many long, rodlike macromolecules such as tobacco mosaic virus,[59, 60] poly(benzyl-L-glutamate),[13–15] and DNA[61] are lyotropic liquid crystals, the absence of birefringence from nanofiber solutions in bromoform not sheared was a surprise to us initially. This was probably caused by the structural difference between the nanofibers and those species studied previously. The nanofibers are not really "hard rods", which are repulsive only in their mutual interactions. At sufficient low nanofiber concentrations, the nanofibers are mutually repulsive because of the osmotic forces acting on the PS chains.[62] At high nanofiber concentrations, the PS chains of different nanofibers may interpenetrate into and entangle with one another. The entanglement should slow down or kinetically impede the self-ordering of the nanofibers. It is only upon shearing that

the nanofibers align. This slow nanofiber motion also explains why the birefringence did not reappear after a sample heated above its order–disorder transition temperature was cooled down again. A further study should involve annealing nanofiber solutions slightly below the order–disorder transition temperature for a long time to see if the birefringence redevelops.

Shear-induced ordering is well known. Cylindrical micelles of small-molecule surfactants form nematic phases in water at weight fractions typically $>30\,\%$.[17, 63, 64] Under shearing, they align along the shearing direction at concentrations as low as $0.1\,\%$.[55, 65] Similarly, the cylindrical domains formed in a diblock melt can be aligned to form "single crystals" by shearing[66–69] or electric forces.[70]

Banded texture: The polarized optical microscopic (POM) image of Figure 12 shows a banded texture. This has also been observed in many other sheared lyotropic or thermotropic liquid crystalline polymer systems.[71–76] The banded textures were seen in polymer systems because of an optical effect caused by the switching in polymer chain orientation from one band to another. While the average chain orientation is along the direction normal to the bands, the chain orientation from one band to another deviates positively and negatively from the average direction.[77, 78] Such nematic phases with banded textures are unique[79] and particularly common[80] for main-chain liquid crystalline or rigid-rod polymers. This is because polymers have large splay constants or it is energetically unfavorable for rigid-rod chains to align in a fan-out fashion.[79] The observation of the banded texture in the nanofiber solution suggests the alignment of the nanofibers along the shearing direction and that the nanofibers behave similarly to rodlike macromolecules[59, 60] and hairy rods.[13–15]

Temperature dependence of the critical concentration for liquid crystalline phase formation: Figure 14 clearly shows that the order–disorder transition temperature increases with nanofiber concentration in bromoform. This temperature dependence seems to make sense intuitively. As the nanofiber concentration increases, the PS chains get more entangled with one another and the nanofiber mobility decreases. A higher temperature will be required to randomize the nanofibers.

This temperature dependence is, however, not predicted by existing theories[57, 58] that consider "hard" or semi-flexible "hard" rods. The temperature dependence is absent in these cases because the rods do not have any other energetic interactions, as two rods can never penetrate one another owing to their physical volume. Our nanofibers are obviously not wormlike hard rods.

Conclusion

The PCEMA block of a PS-*b*-PCEMA sample has been shown by TEM to form cylinders dispersed in the continuous phase of PS when annealed at $110\pm2^{\circ}$C. The SAXS data indicates that the cylinders lie preferentially in the polymer disk plane. The PCEMA cylinders were cross-linked by photolysis. Separating the cross-linked PCEMA cylinders by dissolving PS in THF or toluene yielded isolated nanofibers with PCEMA cores and PS shells. The nanofibers can be tens of micrometers long. This represents a general method for nanofiber preparation from block copolymers.

The nanofibers were soluble in a wide range of solvents including THF, toluene, chloroform, and bromoform. Light-scattering studies in toluene or chloroform revealed that they were wormlike and had molar masses exceeding $10^{10}\,\mathrm{g\,mol^{-1}}$, a persistence length of ~400 nm, and a radius of ~43 nm. They formed lyotropic liquid crystalline phases with a banded texture under shearing above a critical weight fraction, as observed under a polarized optical microscope. The liquid crystals underwent an order–disorder transition at a critical temperature. The order–disorder transition temperature increased with nanofiber concentration in bromoform.

Acknowledgment

G.L. and J.T.G. thank the Natural Sciences and Engineering Research Council of Canada for financial support. G.L. also thanks the Institute for Chemical Science and Technology for financing the early research in this project. B.P.D. was jointly supported by grants to J.T.G. and G.L.

[1] G. Liu, L. Qiao, A. Guo, *Macromolecules* **1996**, *29*, 5508–5510.
[2] G. Liu, *Adv. Mater.* **1997**, *9*, 437.
[3] H. Hasegawa, T. Hashimoto, in *Comprehensive Polymer Science*, *Second Supplement* (G. Allen, S. L. Aggarwal, S. Russo, eds.), Pergamon, London, **1996**, pp. 497–539..
[4] A. K. Khandpur, S. Förster, F. S. Bates, I. W. Hamley, A. J. Ryan, W. Bras, K. Almdal, K. Mortensen, *Macromolecules* **1995**, *28*, 8796.
[5] M. W. Matsen, F. S. Bates, *Macromolecules* **1996**, *29*, 1091.
[6] P. Price, *Pure Appl. Chem.* **1983**, *55*, 1563.
[7] L. Zhang, A. Eisenberg, *Science* **1995**, *268*, 1728.
[8] J. Tao, S. Stewart, G. Liu, M. Yang, *Macromolecules* **1997**, *30*, 2738.
[9] J. Ding, G. Liu, M. Yang, *Polymer* **1997**, *38*, 5497.
[10] J. Spatz, S. Mössmer, M. Möller, *Angew. Chem.* **1996**, *108*, 1673; *Angew. Chem. Int. Ed. Engl.* **1996**, *35*, 1510.
[11] M. Antonietti, S. Heinz, M. Schimdt, C. Rosenauer, *Macromolecules* **1994**, *27*, 3276.
[12] J. Massey, K. N. Power, I. Manners, M. A. Winnik, *J. Am. Chem. Soc.* **1998**, *120*, 9533.
[13] P. S. Russo, W. G. Miller, *Macromolecules* **1983**, *16*, 1690.
[14] W. G. Miller, C. C. Wu, G. L. Antee, J. H. Rai, K. C. Goebel, *Pure Appl. Chem.* **1974**, *38*, 37.
[15] R. Sakamoto, *Colloid Polym. Sci.* **1984**, *262*, 788.
[16] A. Schmidt, S. Lehmann, M. Georgelin, G. Katana, K. Mathauer, F. Kremer, K. Schmidt-Rohr, C. Boeffel, G. Wegner, W. Knoll, *Macromolecules* **1995**, *28*, 5487.
[17] See, for example, W. M. Gelbart, A. Ben-Shaual, *J. Phys. Chem.* **1996**, *100*, 13169, and references therein.
[18] W. Watt, *Philos. Trans. R. Soc. Lond. A* **1980**, *294*, 407.
[19] S. Yajima, *Philos. Trans. R. Soc. Lond. A* **1980**, *294*, 419.
[20] P. M. Ajayan, O. Stephan, Ph. Redlich, C. Collex, *Nature* **1995**, *375*, 564.
[21] B. H. Kear, P. R. Strutt, *Nav. Res. Rev.* **1994**, *46*, 4.
[22] G. M. Chow, K. E. Gonsalves, "Nanotechnology—Molecularly Designed Materials" *ACS Symposium Ser.* **1996**, *622*.
[23] H. Dai, E. W. Wong, Y. Z. Lu, S. Fan, C. M. Lieber, *Nature* **1995**, *375*, 769.
[24] E. W. Wong, B. W. Maynor, D. B. Luke, C. M. Lieber, *Chem. Mater.* **1996**, *8*, 2041.
[25] N. M. Rodriguez, M. S. Kim, R. T. K. Baker, *J. Phys. Chem.* **1994**, *98*, 13108.
[26] S. Iijima, *Nature* **1991**, *354*, 56.

  0947-6539/99/0509-2748 $ 17.50+.50/0

[27] A. Thess. R. Lee, P. Nikolaev, H. Dai, P. Petit, J. Robert, C. Xu, Y. H. Lee, S. G. Kim, A. G. Rinzler, D. T. Colbert, G. E. Scuseria, D. Tomanek, J. E. Fischer, R. E. Smalley, *Science* **1996**, *273*, 483.
[28] N. G. Chopra, R. J. Luyken, K. Cherey, V. H. Crespi, M. L. Cohen, S. G. Louie, A. Zettl, *Science* **1995**, *269*, 966.
[29] W. Han, S. Fan, Q. Li, Y. Hu, *Science* **1997**, *277*, 1287.
[30] A. M. Morales, C. M. Lieber, *Science* **1998**, *279*, 208.
[31] C. R. Martin, *Science* **1994**, *266*, 1961.
[32] D. H. Reneker, I. Chu, *Nanotechnology* **1996**, *7*, 216.
[33] X. Fang, D. H. Reneker, *J. Macr. Mol. Sci. Phys.* **1997**, *B36*, 169.
[34] C. K. Smith, G. Liu, *Macromolecules* **1996**, *29*, 2060.
[35] A. Guo, J. Tao, G. Liu, *Macromolecules* **1996**, *29*, 2487.
[36] J. Tao, A. Guo, G. Liu, *Macromolecules* **1996**, *29*, 1618.
[37] T. Hashimoto, S. Okamoto, K. Saijo, K. Kimishima, T. Kume, *Act. Polym.* **1995**, *46*, 463.
[38] D. R. Lide, *Handbook of Chemistry and Physics*, 76th ed. CRC, Boca Raton, **1995**.
[39] J. Brandrup, E. H. Immergut, *Polymer Handbook*, 3rd ed., Wiley, New York **1989**.
[40] We thank Prof. X. X. Zhu of the University of Montreal for determining the glass transition temperature of PCEMA.
[41] T. Hashimoto, T. Kawamura, M. Harada, H. Tanaka, *Macromolecules* **1994**, *27*, 3063.
[42] M. Shibayama, T. Hashimoto, *Macromolecules* **1986**, *19*, 740.
[43] M. Kato, T. Ichijo, K. Ishii, M. Hasegawa, *J. Polym. Sci.*, *Part A: Polym. Chem*. **1971**, *9*, 2109.
[44] J. E. Guillet, *Polymer Photophysics and Photochemistry—An Introduction to the Study of Photoprocesses in Macromolecules*, Cambridge University Press, Cambridge (UK), **1985**.
[45] J. Tao, G. Liu, J. Ding, M. Yang, *Macromolecules* **1997**, *30*, 4084.
[46] J. Ding, G. Liu, *Chem. Mater.* **1998**, *10*, 537.
[47] G. Liu, X. Xu, K. Skupinska, N. Hu, H. Yao, *J. Appl. Polym. Sci.* **1994**, *53*, 1699.
[48] G. Liu, J. Ding, *Adv. Mater.* **1998**, *10*, 69.
[49] G. Liu, J. Ding, A. Guo, *Macromolecules* **1997**, *30*, 1851.
[50] See, for example, K. S. Schmitz, *An Introduction to Dynamic Light Scattering by Macromolecules*, Academic Press, Boston, **1990**.
[51] Y. Takenao, H. Yamakawa, *Macromolecules* **1980**, *13*, 1518.
[52] P. Sharp, V. A. Bloomfield, *Biopolym.* **1968**, *6*, 1201.
[53] J. S. Pedersen, P. Schurtenberger, *Macromolecules* **1996**, *29*, 7602.
[54] G. Jerke, J. S. Pedersen, S. U. Egelhaaf, P. Schurtenberger, *Phys. Rev. E.* **1997**, *56*, 5772.
[55] M. Y. Lin, H. J. M. Hanley, S. K. Sinha, G. C. Straty, D. G. Peiffer, M. W. Kim, *Phys. Rev. E.* **1996**, *53*, 4320.
[56] G. Porod, in *Small Angle X-ray Scattering* (Eds.: O. Glatter, O. Kratky), Academic Press, New York, **1982**.
[57] L. Onsager, *Ann. N. Y. Acad. Sci.* **1949**, *51*, 627.
[58] A. N. Semenov, A. R. Kokhlov, *Sov. Phys. Usp. Engl. Trans.* **1988**, *31*, 988.
[59] S. Fraden, G. Maret, D. L. D. Caspar, R. B. Meyer, *Phys. Rev. Lett.* **1989**, *63*, 2068.
[60] P. A. Bunning, A. P. Philipse, H. N. W. Lekkerkerker, *Langmuir* **1994**, *10*, 2106.
[61] A. A. Brian, H. L. Frisch, L. S. Lerman, *Biopolymers* **1981**, *20*, 1305.
[62] S. Milner, *Science* **1991**, *251*, 905.
[63] V. Shmitt, F. Lequeux, A. Pousse, D. Roux, *Langmuir* **1994**, *10*, 955.
[64] V. K. Jindal, J. Kalus, H. Pilsl, H. Hoffmann, P. Lindner, *J. Phys. Chem.* **1990**, *94*, 3129.
[65] R. Makhloufi, J. P. Decruppe, A. Ait-Ali, R. Cressely, *Europhys. Lett.* **1995**, *32*, 253.
[66] H. H. Winter, D. B. Scott, W. Gronski, S. Okamoto. T. Hashimoto, *Macromolecules* **1993**, *26*, 7236.
[67] G. Hadziioannou, A. Mathis, A. Skoulios, *Colloid Polym. Sci.* **1979**, *257*, 136.
[68] T. Pakula, K. Saijo, H. Kawai, T. Hashimoto, *Macromolecules* **1985**, *18*, 1294.
[69] K. Almdal, K. A. Koppi, F. S. Bates, K. J. Mortensen, *Macromolecules* **1992**, *25*, 1743.
[70] T. L. Morkved, M. Lu, A. M. Urbas, E. E. Ehrichs, H. M. Jaeger, P. Mansky, T. P. Russell, *Science* **1996**, *273*, 931.
[71] W. Song, S. Chen, Y. Jin, R. Qian, *Liq. Cryst.* **1995**, *19*, 549.
[72] G. Kiss, R. S. Porter, *Mol. Cryst. Liq. Cryst.* **1980**, *60*, 267.
[73] G. Narrucci, N. Grizzuti, A. Buozaurio, *Mol. Cryst. Liq. Cryst.* **1987**, *153*, 263.
[74] E. Marsano, L. Carpaneto, A. Ciferri, *Mol. Cryst. Liq. Cryst. B* **1988**, *155*, 267.
[75] R. Qian, S. Chen, *Makromol. Chem. Macromol. Symp.* **1992**, *53*, 345.
[76] P. Navard, *J. Polym. Sci. Polym. Phys.* **1986**, *24*, 435.
[77] S. Chen, W. Song, Y. Jin, R. Qian, *Liq. Cryst.* **1993**, *15*, 247.
[78] W. Wang, G. Lieser, G. Wegner, *Macromolecules* **1994**, *27*, 1027.
[79] S. J. Picken, P. Moldenaers, S. Berghmans, J. Mewis, *Macromolecules* **1992**, *25*, 4759.
[80] See, for example, W. Wang, G. Lieser, G. Wegner, *Liq. Cryst.* **1993**, *15*, 1.

Received: December 28, 1998 [F 1511]